AFRL-SN-RS-TR-2000-145
In-House Report
October 2000

SPARSE ARRAY ANTENNAS AND CLUTTER SUPPRESSION PROCESSING FOR SPACE-BASED RADARS

Roy P. Basler

APPROVED FOR PUBLIC RELEASE; DISTRIBUTION UNLIMITED.

AIR FORCE RESEARCH LABORATORY
SENSORS DIRECTORATE
ROME RESEARCH SITE
ROME, NEW YORK

Although this report references limited documents (*), listed on page 26, no limited information has been extracted.

This report has been reviewed by the Air Force Research Laboratory, Information Directorate, Public Affairs Office (IFOIPA) and is releasable to the National Technical Information Service (NTIS). At NTIS it will be releasable to the general public, including foreign nations.

AFRL-SN-RS-TR-2000-145 has been reviewed and is approved for publication.

APPROVED:

GERARD J. GENELLO
Project Engineer

FOR THE DIRECTOR:

ROBERT G. POLCE, Chief
Rome Operations Office
Sensors Directorate

If your address has changed or if you wish to be removed from the Air Force Research Laboratory Rome Research Site mailing list, or if the addressee is no longer employed by your organization, please notify AFRL/SNRT, 26 Electronic Pky, Rome, NY 13441-4514. This will assist us in maintaining a current mailing list.

Do not return copies of this report unless contractual obligations or notices on a specific document require that it be returned.

REPORT DOCUMENTATION PAGE			Form Approved OMB No. 0704-0188

1. AGENCY USE ONLY *(Leave blank)*	2. REPORT DATE	3. REPORT TYPE AND DATES COVERED
	October 2000	IN-HOUSE Jun 99 - Jun 00

4. TITLE AND SUBTITLE
SPARSE ARRAY ANTENNAS AND CLUTTER SUPPRESSION PROCESSING FOR SPACE-BASED RADARS

5. FUNDING NUMBERS
PE - 61102F
PR - 2304
TA - E8
WU - 00

6. AUTHOR(S)
Roy P. Basler

7. PERFORMING ORGANIZATION NAME(S) AND ADDRESS(ES)
Air Force Research Laboratory/SNRT
26 Electronic Pky
Rome NY 13441-4514

8. PERFORMING ORGANIZATION REPORT NUMBER
AFRL-SN-RS-TR-2000-145

9. SPONSORING/MONITORING AGENCY NAME(S) AND ADDRESS(ES)
Air Force Research Laboratory/SNRT
26 Electronic Pky
Rome NY 13441-4514

10. SPONSORING/MONITORING AGENCY REPORT NUMBER
AFRL-SN-RS-TR-2000-145

11. SUPPLEMENTARY NOTES
Air Force Research Laboratory Project Engineer: Gerard J. Genello, SNRT, (315)330-3576

12a. DISTRIBUTION AVAILABILITY STATEMENT
Approved for public release; distribution unlimited.

12b. DISTRIBUTION CODE

13. ABSTRACT *(Maximum 200 words)*

Future intelligence, surveillance, and reconnaissance (ISR) missions for the US Air Force are expected to require data from space-based radar (SBR) systems. Several types of data will be needed, including ground-moving-target indicator (GMTI) and airborne-moving-target indicator (AMTI) data. SBR design concepts that are best able to provide these different types of data are still evolving. Space-array antennas and special signal processing techniques are shown here to be capable of achieving useful performance for both GMTI and AMTI applications. Sparse-array patterns for elements at arbitrary (but known) positions are computed by summing the complex vector fields that are functions of the path length difference of each element from the center of the array for azimuth and elevation steer directions of interest. The narrow beamwidths achievable with sparse arrays do not change the clutter power-spectral-density (Cpsd) significantly because the reduced clutter power from each range-azimuth resolution cell is offset by the correspondingly smaller Doppler spread in the cell. Thus the minimum detectable velocity (MDV) of the moving targets is controlled mostly by the pattern of the sub-arrays that are used as elements for the receiving array. For this reason, additional space-time adaptive processing (STAP) must be performed to achieve operationally useful GMTI and AMTI results. A new technique, called main-beam phase compensated aperture (MPCA) processing, is described and evaluated in this paper. When combined with the beamforming processing associated with a phased-array antenna in any configuration, MPCA is shown to result in estimates of SBR performance that are very promising.

14. SUBJECT TERMS	15. NUMBER OF PAGES
Antenna arrays, STAP, clutter suppression, sparse arrays, SBR	34
	16. PRICE CODE

17. SECURITY CLASSIFICATION OF REPORT	18. SECURITY CLASSIFICATION OF THIS PAGE	19. SECURITY CLASSIFICATION OF ABSTRACT	20. LIMITATION OF ABSTRACT
UNCLASSIFIED	UNCLASSIFIED	UNCLASSIFIED	UL

1. INTRODUCTION

Future intelligence, surveillance, and reconnaissance (ISR) missions for the U. S. Air Force are expected to require data from space-based radar (SBR) systems. Several types of data will be needed, including ground-moving-target indicator (GMTI) and airborne-moving-target indicator (AMT) data. SBR design concepts that are best able to provide either or both of these different types of data are still evolving. This report contains the results of a study to show how sparse-array antennas and special signal processing techniques can be applied to achieve the necessary SBR performance for GMTI and AMTI applications.

Sparse arrays in space are attractive for a number of reasons. They can provide the very high angular resolution in both azimuth and elevation that is essential for accurate target tracking at the very long ranges involved. In addition, they are inherently well suited to a modular approach to system design that uses identical relatively small independent spacecraft as sub-arrays. Such spacecraft would permit the SBR to be deployed and tested incrementally, and any failure of an individual spacecraft would cause only a marginal degradation of performance of the overall system. Likewise, the fractional cost impact of an individual component failure would be small.

Unfortunately, any SBR that is not in geo-stationary earth orbit (GEO) receives spread-Doppler clutter from the earth because of its orbital motion and the rotation of the earth. Although a variety of space-time adaptive processing (STAP) techniques might be used by an SBR to deal with spread-Doppler clutter, a new technique that is both simple and effective is described and evaluated in this report. This main-beam phase-compensated aperture (MPCA) processing technique can be considered to be a version of the previously developed $\Sigma\Delta$-STAP method (Ref. 1). This report shows that MPCA, in combination with the beam-forming processing associated with a sparse-array antenna, results in estimates of SBR performance that are very promising.

2. STRAWMAN SYSTEM CONCEPT

Traditional SBR concepts (Ref. 2) have been configured with a phased-array antenna aperture pointed at the nadir. For these concepts, beam steering over roughly ± 60° (depending on SBR altitude) could then provide essentially instantaneous coverage over a relatively large portion of the earth's surface, and thus they were well suited to missions requiring global surveillance. However, the outer portion of the coverage area, where the magnitude of the steering angle is greater than about 30°, is the region of best radar performance, especially because the target radial velocity is sharply reduced near the nadir. In this region of primary interest, up to half of the effective antenna aperture directed toward the nadir is wasted, so the $G_T G_R$ product in the radar equation is reduced by up to 6 dB. Thus, as a starting point for this study, we have made some specific assumptions to permit an evaluation of system performance of a more optimum design.

We assume the SBR mission is not global, but is to provide surveillance of a particular theater of military operations. For optimum resource utilization, we thus assume that the antenna aperture is broadside to the center of the theater when it appears at 15° below the limb of the earth during a given orbital pass. To achieve this broadside orientation, the antenna aperture would need to be mechanically steered after each pass to be ready for the next pass. For purposes of illustration in this report, this mechanical orientation is set so the boresight of the antenna aperture is at right angles to the orbital velocity vector and 15° below the limb of the earth on the right side of the velocity vector.

2.1 Assumptions

(1). Circular polar orbit at an altitude (h) of 1000 km.

(2). The radar will be made up of 16 components, each of which will include a square planar sub-array of antenna elements attached to individual T/R modules. The basic building block of the radar will be a 2-m x 2-m sub-array boresighted normal to the orbit at a depression angle (Δ) of 15° below the horizon (the limb of the earth). These multiple sub-arrays will fly as a constellation of independent spacecraft in any spatial relationship, including contiguous. The radar will operate as a frequency hopping X-band system with a 10 percent hopping bandwidth centered on a frequency of 9.7 GHz, for which the wavelength (λ) is 3.093 cm. The modulation bandwidth will be 10 MHz, so the nominal range resolution will be 15 m.

(3). The mission of the radar will be GMTI and AMTI surveillance of a theater of operations with a nominal extent of 1000 km along the orbit and 235 km or more transverse to it. This area on or near the surface of the earth will be off to the right side of the orbit (relative to the orbital velocity vector).

(4). The coherent integration time (CIT) of the radar will be 25 ms on a given fixed frequency. The inverse of this CIT defines the noise bandwidth as 40 Hz. The pulse repetition frequency (PRF) will generally be about 40960 Hz to give 1024 pulses in a CIT. The PRF will be dithered somewhat to permit range ambiguities to be resolved when necessary (depending on the range to the target, which in turn depends on the antenna beam pointing direction and the

orbital altitude). The PRF will also be reduced whenever necessary to eliminate range ambiguities in the receiving antenna elevation beamwidth projected on the earth.

2.2 Geometry and Coverage

The following are the important implications of the above assumptions with regard to geometry and coverage. Figure 1 shows the basic coverage geometry.

(1). The range (R_1) from the radar to the horizon (the limb of the earth) is $R_1 = (2Reh+h^2)^{1/2} = 3708$ km, and the angle (θ) from the nadir to the horizon is given by $\theta = \arccos(R_1/(Re+h)) \approx 60°$ for a typical radius of the earth (Re) of 6375 km..

(2). The orbital velocity $v = (GM/(Re+h))^{1/2} = 7.35$ km/s for $GM = 3.986 \times 10^5$ km^3/s^2. The orbital period is $2\pi(Re+h)/v = 104.5$ minutes.

(3). The range (R) from the radar to the surface of the earth at a depression angle Δ below the horizon (the limb of the earth) is obtained from the law of cosines, which gives

$$R^2 - 2R(Re+h)\cos(\theta-\Delta) + 2Reh + h^2 = 0.$$

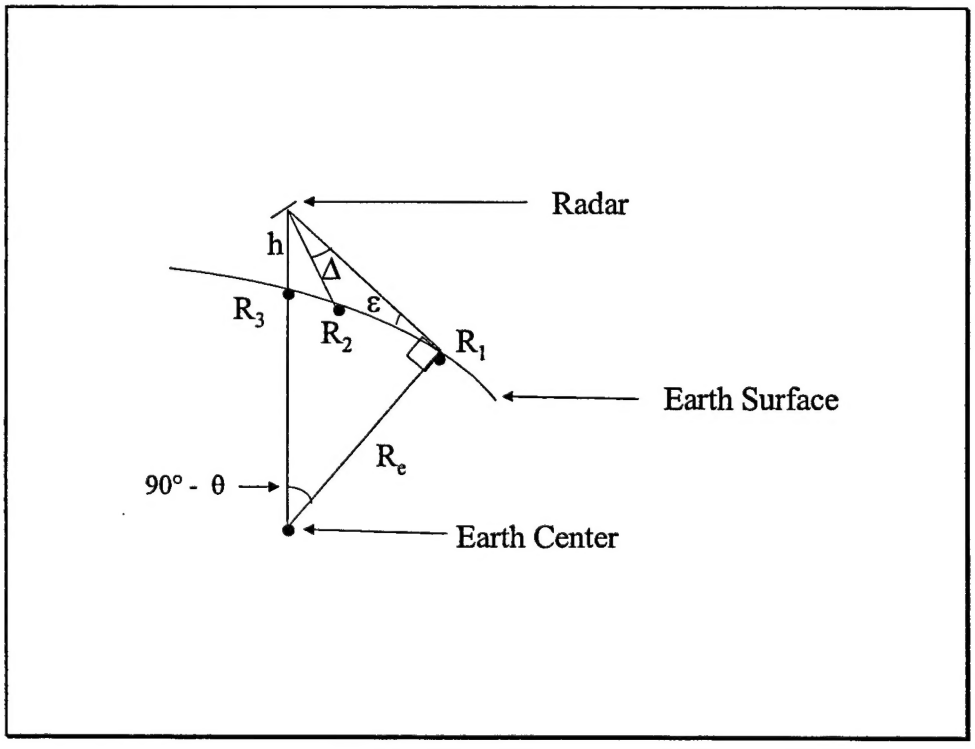

Figure 1. SBR Coverage Geometry.

If we define the boresight depression angle as $\Delta_0 = 15°$, this expression yields $R_2 = 1541$ km for $\Delta = \Delta_0$, and $R_3 = 1184$ km for $\Delta = \Delta_0 + 15°$ (i. e., 30° below the horizon). If we define the azimuth angle relative to the sub-array boresight (which is perpendicular to the orbital velocity

vector) as ϕ, and the orthogonal off-boresight angle in the elevation plane as δ, it will be convenient to describe points where targets are located in terms of the (R,δ,ϕ) coordinate system. Of course, $\delta = \Delta_0 - \Delta$, and $\delta = \Delta_0 - \theta + \theta p$, where $\theta p = \theta - \Delta$, is the angle from the nadir to the point (R,δ,ϕ). Thus, at $(R_1,15°,0°)$ the target will be on the horizon (at the limb of the earth) at $R_1 = 3708$ km, and at $(R_3,-15°,0°)$ it will be at a range $R_3 = 1184$ km, as calculated above. The azimuth angle ϕ will be defined as negative toward the orbital velocity direction (to the left of boresight).

(4). A target that is seen at $(R_2,0°,0°)$ will have appeared on the horizon (it will rise) at $(R_1,0°,-15°)$ and it will disappear (set) about 6 minutes later at $(R_1,0°,15°)$. These values of ϕ and δ at target rise and set and the duration of visibility are approximate. The ranges of the steer angles required for the phased arrays are thus $\pm$ 15° in the vertical (δ) plane and $\pm$ 15° in the horizontal (ϕ) plane. The fraction of the earth's surface contained in this solid angle of radar coverage is about 1% at any given instant.

(5). At boresight, the radar signal arrives at the surface of the earth at $(R_2,0°,0°)$ at an elevation (grazing) angle (ε) of about 35°, because in general, $\sin\varepsilon = \cos\theta p$, and

$$\sin\varepsilon = (2R_e h + h^2 - R^2)/(2RR_e)$$

At the horizon (the limb of the earth), that is at $(R_1,15°,0°)$, $\varepsilon = 0°$, and at $(R_3,-15°,0°)$, $\varepsilon \approx 55°$. At the nadir, $\delta = -(\theta - \Delta) \approx -45°$, so at (1000km,-45°,0°), $\varepsilon = 90°$. A nominal Tx beamwidth of 1° would illuminate a spot on the surface of the earth that is stretched along the beam by a factor of $1/\sin\varepsilon$, so it would have dimensions of about 27 km by 47 km at $(R_2,0°,0°)$, and 21 km by 25 km at $(R_3,-15°,0°)$. At the horizon (the limb of the earth), at $(R_1,15°,0°)$, the cross-beam dimension of the illuminated spot is about 65 km and although the stretching factor theoretically approaches infinity, it is effectively limited to unity because of the earth's curvature.

(6). If we consider the middle of the theater of interest at range R_2 as a representative case, the range to the edge of the theater (500 km to the left or right of the middle) would increase only about 5% above R_2. It would thus take about 37 beam positions in ϕ and 5 in δ, or about 185 beams in total, to completely cover the theater. For the 25-ms cycle time mentioned above, the entire theater could thus be covered by beam scanning in about 5 s.

3. ANTENNA PATTERNS AND CONFIGURATIONS

Antenna patterns for filled arrays with uniformly spaced elements are typically computed using analytic expressions that are valid only because of the symmetry of the array about its center. In particular, the mathematical techniques used to derive these analytic solutions can not be used when elements are not symmetrically paired around the center of the array (Ref. 3). However, for sparse arrays with element positions that may be irregular, or even random, it is necessary to use a direct approach to pattern calculation. To calculate the antenna pattern in this case, the complex vector fields that are functions of the path length difference of each element from the center of the array must be summed for azimuth and elevation steer directions of interest.

3.1 Sub-Arrays

As a starting point for defining a realistic SBR antenna for this study, we have used an array built and tested by Raytheon to validate a concept for SBR applications (Ref. 4). This array consists of 104 circular patch radiating elements on individual T/R modules assembled so the elements form an equilateral triangular grid with a spacing of 0.55 wavelengths at a mid-band frequency of 9.7 GHz. The measured VSWR was below 2:1 over the range 8.98-10.34 GHz, so it can be considered a broadband system. The measured gain of a patch element is about 4.6 dBi at 9.7 GHz, and its pattern varies approximately as the cosine of the off-boresight angle in both the E- and H-planes.

The Raytheon array plane is approximately a square about 17 cm on a side, and one side of each equilateral triangle in the grid is parallel to one side of this square. The 104 T/R modules are arranged in nine rows of six interleaved with ten rows of five, but with the modules in the interleaved rows rotated by 180°. Raytheon demonstrated the array steering over a ± 60° scan volume, which considerably exceeds the ± 15° volume that we require. Each T/R module radiates a peak power of 2-W and could operate at a duty factor of 25 % to give an average power of 0.5-W at mid-band, and at about 20 % and 0.4 W at the band edges.

To check the validity of the computer code developed for direct calculation of antenna patterns, the coordinates of these 104 elements were used to calculate patterns of the Raytheon array as a function of azimuth and elevation angles. These patterns were found to compare very favorably with measured patterns presented by Raytheon.

For purposes of this study, a standard sub-array has been defined as consisting of a square array of 110x110 patch elements with a spacing of 0.55 wavelengths. A square grid is assumed instead of a triangular grid to permit a simple analytic calculation of the sub-array pattern without using the computer code for direct pattern calculation. Uniform weighting is assumed for the sub-array, but for purposes of reducing spread-Doppler clutter, it will be shown that weighting for side-lobe reduction would be advantageous. Although this standard sub-array is referred to as having nominal dimensions of 2-m x 2-m, its actual aperture is only about 1.9 m on a side. The half-power beamwidth of the standard sub-array is 0.838° in both azimuth and elevation, which is smaller than the nominal value of 1° mentioned above in calculating the 5-s

revisit time for theater surveillance. As more appropriate revisit times, we will thus assume that the entire theater could be covered by beam scanning in about 7 s with the standard sub-array.

3.2 Arrays and Patterns

Two configurations of sub-arrays are considered here to illustrate the characteristics of sparse arrays compared to filled arrays. For the filled array, the sub-arrays are arranged as a 2x8 contiguous array with the long dimension along the orbital velocity vector. For the sparse array, the sixteen sub-arrays are randomly distributed over a 200-m by 200-m aperture, with the restriction that no sub-array can be closer than 5 m to any other sub-array (so they will not collide in orbit). This aperture is chosen arbitrarily, simply to illustrate the principles involved. Aside from practical limitations on the SBR-constellation orbit, the optimum size of a sparse aperture will also depend on other tradeoffs, such as between tracking accuracy and the cost of the number of parallel processing channels required for the simultaneous receive-beams needed to cover the transmitter beam.

An example of the element positions for a random array is given in Figure 2. The somewhat awkward labels for the x and y axes in this figure are required because of the definition of the coordinate system with the antenna boresight direction going into the page at (0,0) and with the orbital velocity vector pointing to the left. In other words, the orbital velocity is in the minus-x direction in the figure, corresponding to negative azimuth steer angles. In this orientation, positive azimuth angles are toward the right of the figure and positive elevation angles are to the top. Because these elements are placed at random over a square aperture 200-m on a side, the actual aperture typically is less than 200 m, as is the case for the example shown in the figure. (The x-aperture is the difference between the maximum and minimum x-values, and likewise for the y-aperture.)

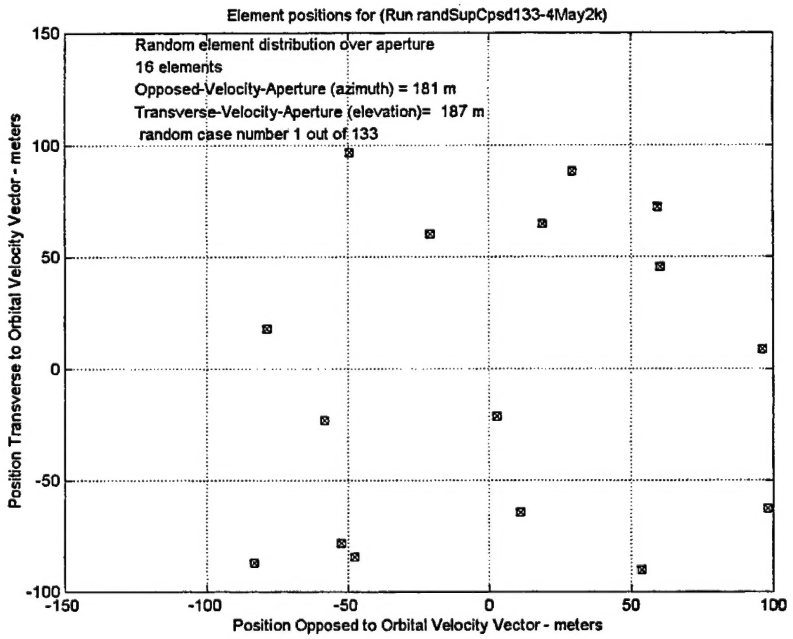

Figure 2. Example of element positions for a random sparse array.

In practice, random arrays of N elements are generated for this study by assigning random coordinates (x_i,y_i), to the i^{th} element, where x_i lies within a specified opposed-velocity aperture and y_i lies within a separately specified transverse-velocity aperture. After the initial assignment, the coordinates are transformed (translated) to define the origin as the array center at $x_0 = (\Sigma x_i)/N$ and $y_0 = (\Sigma y_i)/N$. N can be any integer, but it is sixteen for the examples presented in this report. This same practice could easily be followed in orbit. Continuous real-time laser range-finder measurements could be made of the distance from each sub-array to each of the other sub-arrays. These data could then be processed to define the origin of the SBR coordinate system as the center of the constellation of sub-arrays at every instant.

Figure 3 shows the azimuth patterns of the random sparse array from Figure 2 and of the 2x8 contiguous array. These are G_TG_R patterns, so the sub-array pattern is squared because it constitutes the entire transmit pattern, and it is also part of the receive pattern. The elevation-pattern comparison for these same two arrays is shown in Figure 4, and it differs from the azimuth comparison primarily in that the pattern for the 2x8 array reflects the fact that the elevation aperture is only a quarter the size of the azimuth aperture.

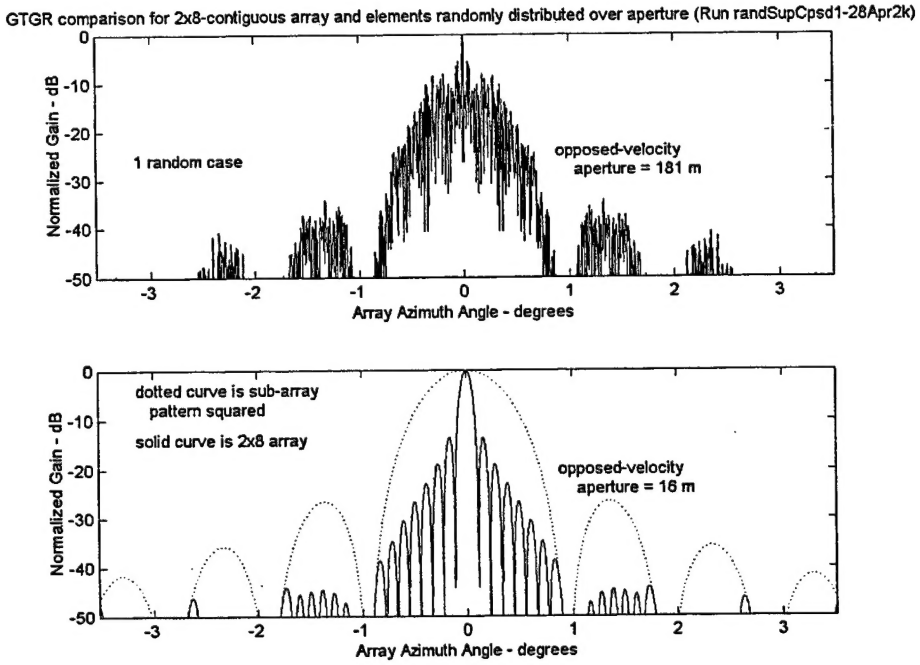

Figure 3. Azimuth patterns of a random sparse array and the 2x8 contiguous-array.

The azimuth patterns of the filled 2x8-array and 133 different random sparse arrays are compared in Figure 5. The curves for the random patterns in this figure do not correspond to any of the 133 actual patterns computed, but instead show how the patterns are distributed statistically. It can be seen in these figures that the sub-array pattern dominates the shapes of the array patterns outside the main lobe. However, within the main lobe the advantage of the narrow beamwidth of the sparse array is somewhat offset by its higher grating lobes compared to the regular sidelobes of the filled array. Nevertheless, the entire feasibility of sparse arrays for SBR applications is dependent on the effectiveness of the sub-array pattern to suppress the

contributions of the full-array grating-lobes outside its main beam. It is also important that the patterns of random sparse arrays are generally as good as or better than the pattern of any non-random placement of elements that might be contrived.

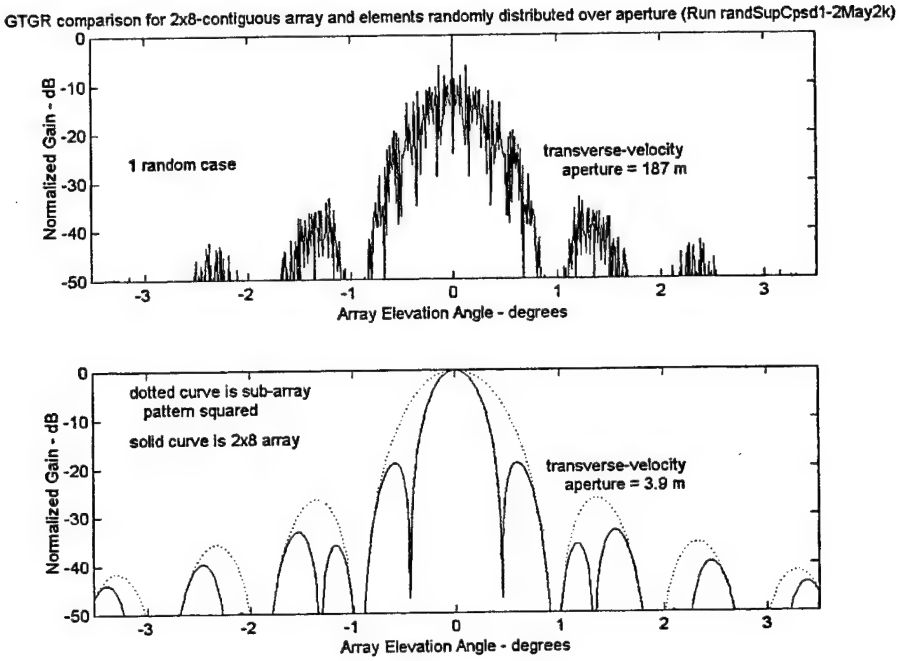

Figure 4. Elevation patterns of a random sparse array and the 2x8 contiguous-array.

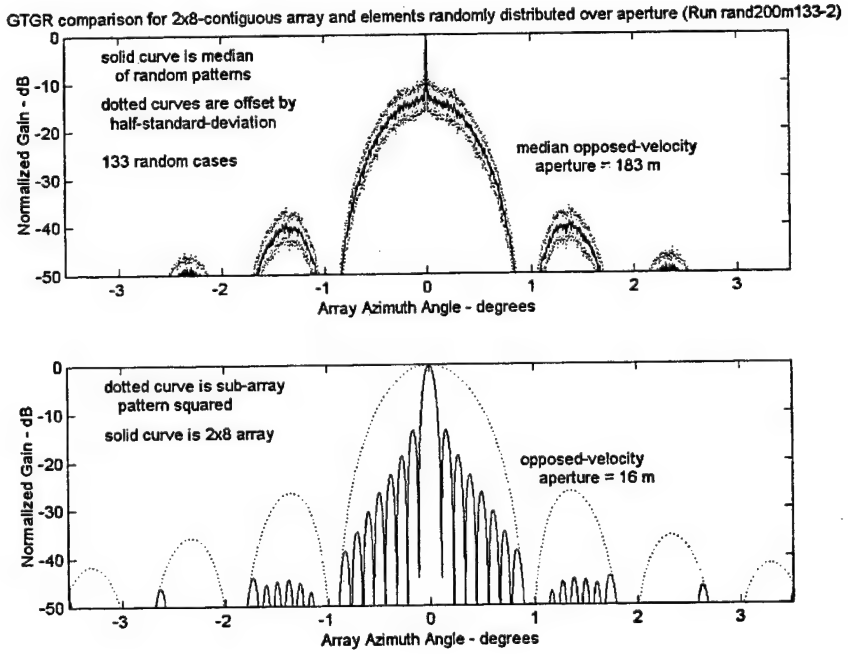

Figure 5. (U) Azimuth patterns for 133 random sparse arrays and the 2x8 filled array.

Even within the main lobe of the sub-arrays, grating lobes should not be considered a serious problem because they will appear at different angles when the radar hops to a different frequency. Thus if two or more successive dwells are scheduled on different frequencies at the same steer angle, the spurious sidelobe target will appear in only one of them. These patterns are shown only for angles between about ± 3.5°, but they continue to decrease in the same manner out to larger angles because of the well-behaved sub-array patterns. It is shown in the next section that these patterns with their sidelobe/grating-lobe structure map directly into the Doppler domain of the clutter.

To calculate the pattern for an SBR, the relative positions all of the sub-arrays must be known to an accuracy of better than a millimeter at all times. As mentioned previously, this information can be provided in real time by multiple laser range finders. In addition to this basic distance measurement, each sub-array must be able to make the phase adjustment that will be necessary to steer the array beam to its desired pointing angles during each CIT. Also, the attitude control system of each spacecraft should maintain the boresight of the sub-array so that it is pointed at the center of the theater of interest during each pass. (For the examples presented in this report, this boresight is assumed to be perpendicular to the orbital velocity vector at the designated depression angle of 15° below the horizon (the limb of the earth) viewed to the right of the velocity vector). It will not be necessary for the sub-array boresight pointing directions to be controlled to an accuracy better than about a degree or two, but each must be known at all times to within a small fraction of a degree, which is easily achievable with current space technology.

The spike in the center of the sparse-array curves in Figures 3-5 at 0° azimuth and 0° elevation, and sitting atop the broader peak caused by the sub-array pattern, is the contribution of the main-beam of the array pattern. The height of the spike is determined simply by the number of elements (sub-arrays) in the array, and its width in azimuth and elevation is determined by the array apertures in the opposed-velocity and transverse-velocity directions respectively.

Because the particular spatial distribution of elements over the aperture is of relatively little importance in defining the shape of the main-beam spike, it will not be necessary for the SBR constellation to maintain any particular element positions. It will only be required that the elements roughly fill a sufficiently large aperture. Station keeping requirements for the individual spacecraft can thus be relaxed to permit drifting about within the constellation.

The tiny size of the array pattern spike relative to the underlying sub-array pattern shows that the SBR should not generally be operated coherently for transmitting, that is, with all of the sub-arrays transmitting the same frequency with appropriate phase adjustments to make $G_T = G_R$. The duration of a single orbital pass over the theater would be much too short to permit full theater coverage by beam scanning with such a tiny beam. However, the SBR could operate in this spotlight mode for a few dwells per pass to investigate particular targets or areas of interest, such as traffic choke points like highway intersections or mountain passes, with a very high signal to noise ratio (SNR). This coherent transmitter operation would increase the SNR by 24 dB for configurations with only 16 sub-arrays.

However, an attractive SBR configuration would be to transmit with all sub-arrays, but with each illuminating different but adjacent portions of the theater on a different frequency. This mode of operation would reduce the revisit time to $7/16 \approx 0.44$ s for arrays of 16 standard sub-arrays. These short revisit times would improve the performance of the track-while-scan tracker and/or would permit increasing the CIT to improve the single-dwell SNR.

The elevation beamwidth is about 0.007° and the azimuth beamwidth is about 0.008° for the example in Figure 4. These very small beamwidths would require more than 15,000 parallel receiving/processing channels to provide one for each receiver beam needed simultaneously to cover that transmitter beam completely. This large number could be reduced, of course, by using a larger sub-array, but the time required to scan the Tx beam over the entire theater, and the number of revisits to each portion of the theater during an orbital pass, would then be correspondingly increased. However, the number of sub-arrays could be made smaller to maintain the power-aperture-product ($P_T G_T G_R$) sufficiently unchanged so as not to compromise target detection and tracking. Optimization of an SBR would require a trade-off between the launch costs of a larger sub-array and the hardware costs associated with the receiving/processing channels.

4. SCNR AND MDV WITH CONVENTIONAL DOPPLER PROCESSING

Two useful measures of SBR performance that can be calculated in a straightforward manner from the radar equation are the signal to clutter plus noise ratio (SCNR) and the minimum detectable velocity (MDV). For signal calculations we simply assume a nominal value of 0 dBsm for the radar cross section (σ) of the target. Also, we simply assume that the noise is kTB, as given in terms of Boltzmann's constant (k), with the temperature (T) of the earth's surface set to a representative value of 300 K, and the noise bandwidth (B) is 40 Hz, the inverse of the 25-ms CIT. For arrays made up of the standard sub-array, the average transmitter power (P_T) is $10\log(110^2/2) = 37.8$ dBW because of the 2 W peak power and 25% duty factor of a T/R module at midband. Likewise, the peak of the transmitting antenna gain (G_T) for the standard sub-array at boresight is $4.6 + 10\log(110^2) = 45.4$ dBi, because 4.6 dBi is the patch element gain for each T/R module. Also, the peak of the receiving antenna gain (G_R) is $4.6 + 10\log(110^2) + 10\log(16) = 57.4$ dBi. Of course, the G_TG_R product is reduced at off-boresight angles as shown by the patterns in Figures 3-5. The range to the target to be used in the radar equation is given by the expression for R in Section 2.

To calculate the received clutter power, σ is simply replaced by $\sigma_0 A_c$, where σ_0 is the cross section of the surface of the earth per unit area and the area (A_c) contributing to the clutter is given by $A_c = rRb_{az}\sec\varepsilon$. The size of the range cell (r) is 15 m, b_{az} is the azimuth beamwidth of the receiving antenna, and ε is the (grazing) angle of incidence as defined in Section 2. This expression for A_c is valid only when a single range cell is contained within the receiving antenna beam when it is projected on the earth (Ref. 5). To satisfy this condition, we must reduce the PRF whenever necessary from its standard value of 40.96 kHz (which gives 1024 pulses in the 25-ms CIT), to the maximum value at which no range ambiguities occur within the footprint of the half-power elevation beamwidth.

Clutter is Doppler shifted by a frequency (f_d) because of the spacecraft's orbital velocity and the rotation of the earth (Ref. 5). The clutter power spectral density (Cpsd) is computed as the clutter power divided by the difference between the maximum and minimum f_d within each range-azimuth resolution cell. To compute the Cpsd received by the SBR, it is necessary to specify the latitude and longitude of the target. For purposes of illustration, we have chosen target coordinates of 45° N and 21° E (approximately the location of Belgrade). Cpsd(f_d) is in turn a function of the steer direction of the antenna beam as defined by ϕ and δ, but again for purposes of illustration the elevation angle (δ) is set to 0° for all the plots to be shown here.

It might be noted that our 15-m range cell projected on the earth at 45° N corresponds to an increment of elevation angle of only about 10^{-4} degrees, about two orders of magnitude smaller than the half-power beamwidths of our random sparse arrays. Thus, because the change of f_d with δ and ϕ relative to the size of the Doppler resolution cell B (40 Hz for a CIT of 25 ms) is small compared to the change of R with δ and ϕ relative to the size of our 15-m range cell, no range-Doppler coupling needs to be taken into account in the computation of Cpsd($f_d(\delta,\phi)$). In other words, because we compute $R(\delta,\phi)$ and $f_d(\delta,\phi)$ in angle increments of half a beamwidth or more, the resulting Cpsd(f_d) never has any energy folded into it from other range cells.

Figure 6 shows Cpsd(f_d) as computed for the SBR with the same example of a random sparse array shown in Figures 2-4. The Doppler frequencies plotted in Figure 6 are all unambiguous. Relative to the Cpsd peak, they extend to ±PRF/2, which corresponds to radial velocities of roughly ±300 m/s, so target Doppler frequencies for such an SBR would be unambiguous for most aircraft velocities. The position of the Cpsd peak in Figure 3 is a result of the peak in $G_T G_R$ at $\phi = 0°$, where the component of relative radial velocity of the clutter cell caused by the orbital motion of the SBR is also zero. Of course, the falloff of Cpsd on either side of the peak is because the clutter is reduced by the shape of the antenna pattern at the off-boresight angles as shown in Figure 3. On the other hand, the Doppler frequency is zero at the azimuth angle where the radial component of the clutter-cell relative-velocity due to orbital motion cancels out the component due to the rotation of the earth.

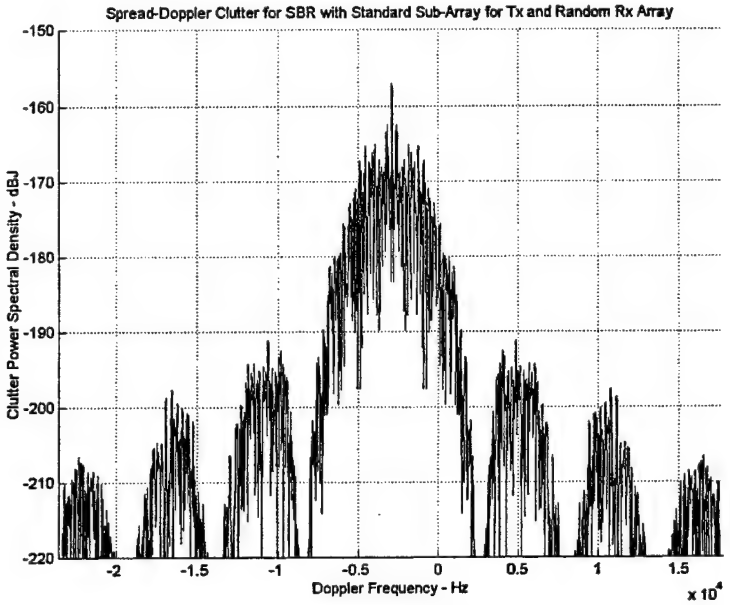

Figure 6. Example of Cpsd for an SBR with a random sparse array.

The Cpsd for the 2x8 contiguous array is shown in Figure 7, and it is plotted over the same range of Doppler frequencies used for the previous figure. However, because of the broad elevation beamwidth of the filled array relative to the sparse array, the PRF for this SBR had to be reduced to 10.88 kHz to avoid range ambiguities at $\delta = 0°$ (the case shown here). Thus, Doppler folding was taken into account for this figure because the Doppler frequencies are unambiguous only out to ±5.44 kHz (relative to the Cpsd peak), which is about where the clutter level reaches the noise level in the first null of the sub-array pattern. Fortunately, because the energy in the sub-array sidelobes is so small relative to that in the main lobe, folding has a negligible on the main-lobe Cpsd. For the 2x8 array, the Cpsd-width away from the central peak is slightly less than it is for the sparse array shown in Figure 5. However, because of Doppler folding, a much smaller fraction of the population of likely aircraft radial-velocities would be outside the main-lobe clutter for the filled array than for the sparse arrays.

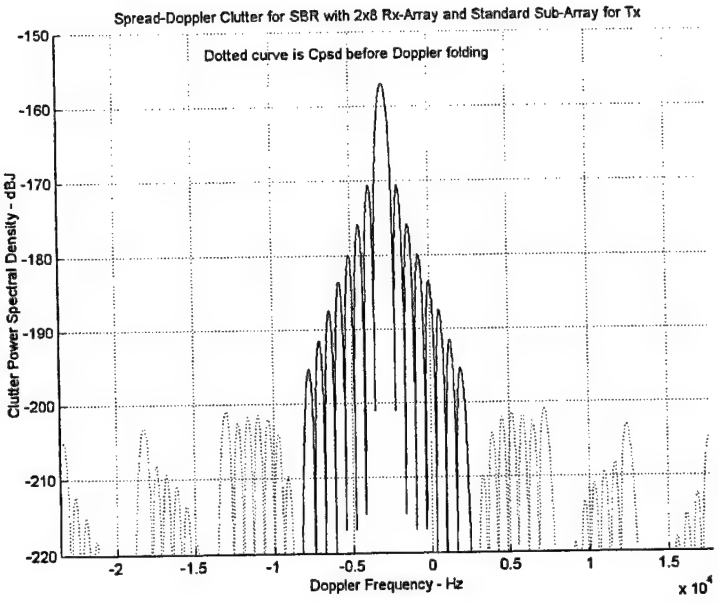

Figure 7. Cpsd calculated for the 2x8 array with Doppler folding.

The energy levels in the Cpsd for the sparse arrays are only slightly smaller that for the filled array in spite of a difference of more than a factor of ten in the azimuth beamwidths (and thus in the respective clutter cross sections). This difference is slight because both the area of the clutter patch and the Doppler spread within it are reduced by comparable amounts for the sparse arrays.

A more revealing presentation of spread-Doppler clutter results is in terms of SCNR and MDV as shown in Figure 8, for which the effects of simple Doppler processing have been taken into account. In particular, a 1024-point Hamming window, corresponding to the length of the CIT in the time domain at the assumed PRF, is zero-padded and Fourier-transformed into the frequency domain to perform a circular-convolution with the 4096 Cpsd-points plotted in Figure 6. The MDV is then determined from points where the SCNR is unity (or 0 dB). This procedure is repeated for each random case to produce the statistical results shown in Figure 8.

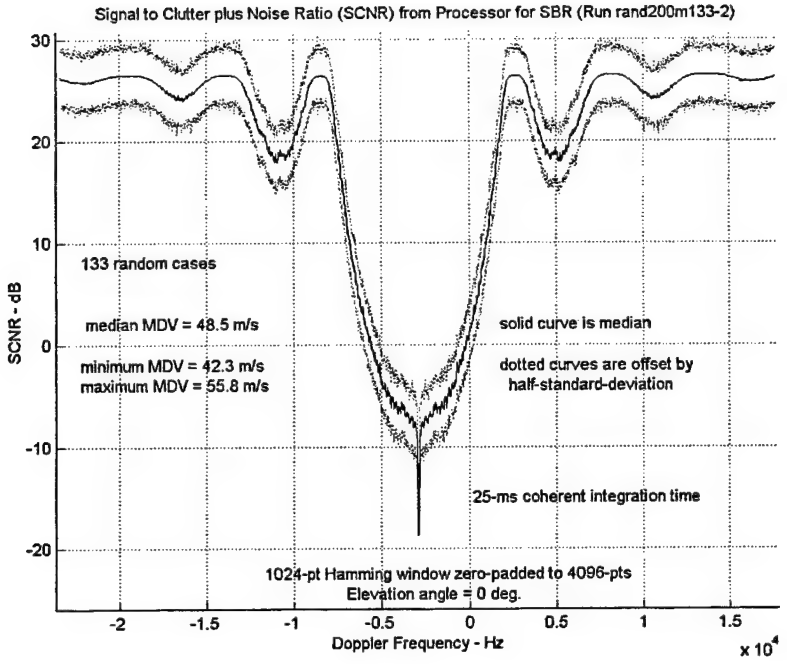

Figure 8. SCNR and MDV for 133 random sparse arrays.

It might be noted that the median MDV listed in Figure 8 does not correspond exactly to where the median SCNR is unity (0 dB). The MDV distribution is orthogonal to the SCNR distribution on this plot in the sense that MDV values are scattered in the horizontal (Doppler) direction whereas the SCNR values are scattered in the vertical direction.

The extent of the Doppler frequency axis in Figures 6-8 corresponds to the values calculated for $\delta = 0°$ and for azimuth angles between about $\pm 3.5°$, as shown in Figure 9. Although $f_d(\phi)$ as shown in Figure 9 appears to be a linear relationship, it is actually a function of $\cos\phi$. The extravagance of displaying this simple one-to-one functional relationship in a figure is to emphasize that it will be critical to the clutter suppression processing described in the next section.

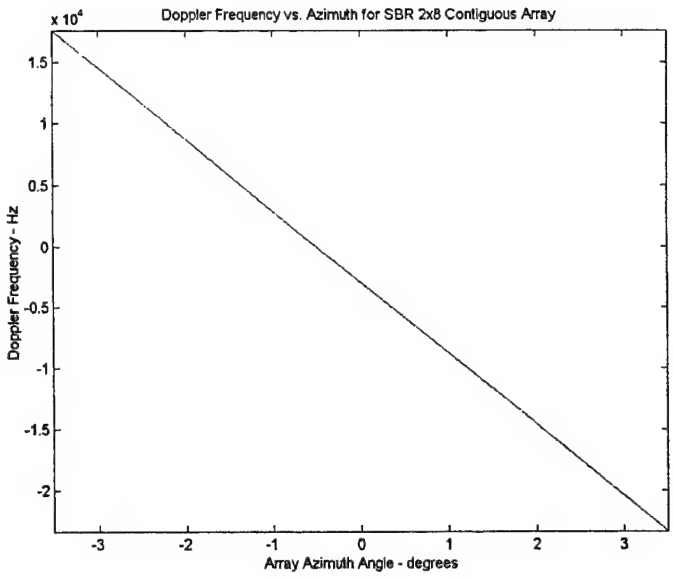

Figure 9. The relation of f_d to ϕ for an SBR target at of 45° N, 21° E.

Although the SCNR and MDV values for all of these SBR cases show a detection capability that would be of some use for AMTI applications, useful GMTI performance and maximum AMTI performance will require additional clutter suppression processing, as described in the next section.

5. CLUTTER SUPPRESSION PROCESSING

The concept of using STAP for clutter suppression with sum and difference beams has been described in a previous publication (Ref. 1). This concept is referred to in general as ΣΔ-STAP, and in this paper we use the acronym MPCA (for main-beam phase-compensated aperture) to refer to a particularly simple and attractive implementation of the general concept. The essential idea of MPCA is that a target signal will appear only in the sum beam whereas clutter appears both in the sum and difference beams. Thus, by suitably weighting each Doppler component of the output of the difference beam and subtracting it from the corresponding component of the sum beam, the clutter is suppressed, but the target signal is unaffected. After subtraction, the target signal will remain with an SCNR and Doppler frequency that depend on its radar cross section and radial velocity. It should then be possible in theory to detect it everywhere except in the Doppler bin corresponding to zero radial velocity, that is, everywhere except in the null of the difference beam that is placed on the peak of the sum beam. This null can be made sharp enough in angle and Doppler frequency for effective performance of the GMTI mission.

The sum beam is formed by combining the complex vector fields from the 16 sub-arrays to form a peak in the desired steer direction (θ_n) as shown in Figure 2 (where θ_n corresponds to $\phi = 0$ and $\delta = 0$). On the other hand, the difference beam must be formed from the same inputs using an optimization procedure that sets a null in the specified steer direction, while maximizing the gain of the antenna array in some other specified direction (θ_0, referred to here as the main beam direction). There are no constraints placed on the location of either the null or the main beam. Sarkar and Strait (Ref. 7) have described a technique based on the Method of Moments to find the optimum weights that maximize the gain in one direction while simultaneously placing nulls in other directions. However, in this paper the far field is obtained using the known steering vectors associated with the directions of the null and the main beam. For maximum clutter suppression, we specify the steer direction for the main beam to be at each value of ϕ corresponding to each Doppler bin contained in the main lobe of the sub-array pattern. Clutter suppression outside this main lobe is best handled by tapering the sub-array for both transmitting and receiving, instead of using the uniform weights employed for the illustrations presented here. The analysis begins by writing the far field response at the null and the main beam as:

$$\begin{bmatrix} E^{ff}(\theta_n) \\ E^{ff}(\theta_0) \end{bmatrix} = \begin{bmatrix} \mathbf{s}^H(\theta_n) \\ \mathbf{s}^H(\theta_0) \end{bmatrix} [\mathbf{v}]$$

where $E^{ff}(\theta_n)$ is the far field in the direction of the desired null and $E^{ff}(\theta_0)$ is the far field in the direction of the desired main beam. $\mathbf{s}(\theta_n)$ represents the steering vector in the direction of the desired null and $\mathbf{s}(\theta_0)$ represents the steering vector in the direction of the desired main beam. The problem thus reduces to minimizing $E^{ff}(\theta_n)$ while simultaneously maximizing $E^{ff}(\theta_0)$. The procedure is similar to that used by Sarkar and Strait (Ref. 7) and modified by Adve (Ref. 8).

By determining the weights (α) for the null beam with its peak at the azimuth angle corresponding to the Doppler bin of interest, we insure in most cases that α is unity or less. These weights from the angle domain can be applied in the Doppler-frequency domain because

of the relationship illustrated in Figure 5. For a few random array configurations, especially near the nulls in the sub-array pattern, the side-lobe and grating-lobe structures of the sum beam and the null beam are such that α is greater than unity. The result for these cases is that the signal-to-suppressed-clutter-plus-noise-ratio (SC_sNR) is less than the theoretical SNR by more than the value of 3-dB that would apply if α were unity. If necessary, these cases with $\alpha > 1$ can be eliminated by judicious choice of radar frequency within its hopping bandwidth for any random array configuration.

After this MPCA processing, the MDV is reduced to about 1 m/s, corresponding to one or two Doppler bins from the minimum of the SCNR shown in Figure 8. For application to real radar data, the weights defined by this theoretical α would be used to combine the actual processor outputs from the Σ and Δ beams to produce a SC_sNR that would reveal the target signals remaining after the clutter is suppressed.

A significant operational advantage would result if a single LEO-SBR system could perform both GMTI and AMTI missions simultaneously using the same transmitters, receivers, antennas and signal processors. MPCA processing would provide such a simultaneous dual capability, so an important next step will be a testing of the MPCA technique using experimental data. If the weights (α) derived from the MPCA method described here are found not to be effective for clutter suppression with experimental data, some other more traditional $\Sigma\Delta$-STAP technique will have to be used to determine α.

6. GEOSYNCHRONOUS SBR

During the cold war, U. S. security required the continuous surveillance of the entire planet, especially for submarine-launched ballistic missiles (SLBMs), intercontinental-ballistic missiles (ICBMs) and long-range bombers. However, now that the cold war is over, the threat that the U. S. Air Force must deal with for the foreseeable future is not global, but is limited to theater-sized areas in a relatively few places such as the Balkans, the Middle East, or Korea. In this situation, what the Air Force needs is an SBR that can perform the missions of both AWACS and JSTARS with lower cost and improved performance. In general, the problem with a surveillance system in low-earth orbit (LEO), or any orbit other than geosynchronous earth orbit (GEO), is that each satellite spends the great majority of its time looking somewhere outside the theater of interest. On the other hand, a GEO-SBR could be positioned to operate only where it is needed.

In particular, the optimum SBR for regional conflicts would provide continuous surveillance of a theater-sized region to perform real-time detection and tracking of all targets of military significance. These targets would include ballistic missiles, aircraft, helicopters, and cruise missiles, in addition to surface vehicles like tanks, transporter-erector-launchers (TELs) for missiles, trucks, trains, and automobiles, and surface ships. If the future threat again evolves to require global surveillance, multiple GEO-SBRs could be deployed to provide it.

6.1 Orbital Perturbations

Satellites in GEO are not actually stationary with respect to the earth because the gravitational pulls of other celestial bodies (mostly the moon and the sun) move them continually over a small region as a perturbation to their orbit. To illustrate the effects of this motion, a GEO-SBR is assumed to be located in the earth's equatorial plane at 26° East Longitude, to provide surveillance of a theater centered on Belgrade.

The SBR state vector (its position and velocity components at one-minute intervals) were calculated using the Satellite Tool Kit® (Ref. 7) for 13 January 2000. The variation of the resulting position components with time are shown in Figure 21, where it can be seen that most of the motion is in the North-South direction. The rotating rectangular coordinate system used here is defined with its origin at the center of the earth. The x axis passes through the equator in the Greenwich meridian plane, the y axis passes through the equator at 75° East Longitude, and the z axis passes through the North and South poles. The oblateness of the earth is taken into account using the expression for Re as a function of latitude (η), namely

$$R_e \text{ (in km)} = 6378(1-(\sin^2\eta/297.3))$$

The mean position given in Figure 21 can be seen to be about 6.61 R_e from the earth's center. The range from the SBR to the theater (R_s) and the grazing angle of incidence (ε) must be obtained by solving the following simultaneous equations defined by the law of sines and the law of cosines

$$R_s/\sin\eta = (x^2+y^2+z^2)^{1/2}/\sin(\varepsilon+\pi/2)$$

$$x^2 + y^2 + z^2 = R_s^2 + R_e^2 - 2\,R_s\,R_e\cos(\varepsilon+\pi/2)$$

For Belgrade, with $\eta = 26°$, $R_s = 37{,}939$ km and $\varepsilon = 38.2°$.

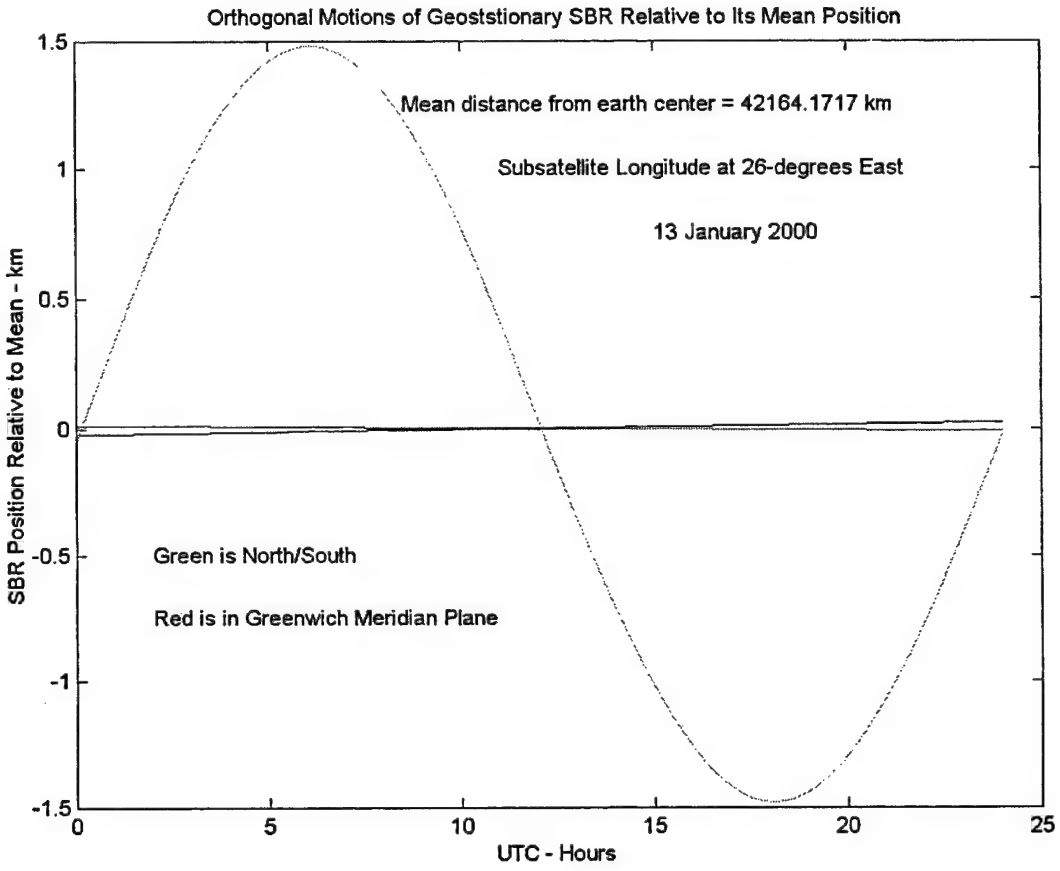

Figure 21. Orthogonal motions of a GEO-SBR relative to its mean position.

It is shown below that these slow orbital perturbations cause negligible spreading of the clutter Doppler spectrum, unlike the previously presented cases for a LEO-SBR.

6.2 VHF/UHF System Concept

The performance capability of a feasible GEO-SBR system is presented here to illustrate the advantages of this orbit over LEO in spite of the greatly increased range to the target. In this case, instead of X-Band, the operating band is chosen to be from 200-400 MHz to take advantage of the larger target cross sections available because of resonant scattering. Also, power amplifiers with average powers of hundreds of Watts are readily available for this band as commercial off-the-shelf items.

The sub-array for the VHF/UHF GEO-SBR is an 8x8 array of crossed log-periodic-antenna (LPA) elements (with a mid-band wavelength of $\lambda = 1$ m), each of which is placed on a square grid with a spacing of 0.55λ. These LPA elements are inherently capable of transmitting with a VSWR of better than 2:1 over the entire 200-400 MHz operating band. The crossed elements will be oriented at an angle of 45° with respect to this grid to facilitate the dense element packing. Each orthogonal component of the crossed LPA will be connected to a power amplifier with an average power of 500 W. Any desired linear or circular polarization will be synthesized by appropriate phasing of the signal transmitted from each LPA. The instantaneous bandwidth of 10 MHz will be hopped over the 200-MHz operating band at intervals of the round-trip propagation time to the surveillance area. All of this round-trip propagation time will be available for coherent integration, so the CIT will be about 285 ms for surveillance of Belgrade. It is convenient to think of the GEO-SBR CIT as about a quarter of a second, which corresponds to a Doppler resolution of about 4 Hz. The system will have separate Tx and Rx antenna arrays, to permit operation as a quasimonostatic radar with unity duty factor. Because of the way the CIT is chosen, the receivers will always be tuned to a different frequency from the one being transmitted.

If a linear polarization is transmitted, it will arrive in the surveillance area with a polarization that is controlled by the Faraday rotation in the ionosphere caused by the integrated electron density along the propagation path. The crossed LPAs in the Rx array will permit synthesis of the optimum polarization required to receive any target signal after its Faraday rotation along the return propagation path. At the same time, this polarization diversity will permit very effective nulling of any jammer signal that may present.

The choice of aperture for the Tx and Rx arrays involves a tradeoff between a number of parameters especially including: the power-aperture product required to give an SNR adequate for target detection; the size of the theater of interest; the minimum revisit time required for effective detection and tracking of the most stressing target; and the number of Rx antenna beams that are considered affordable to cover the Tx beam. To illustrate the potential performance of a GEO-SBR, we assume the following: the theater is a circle with a diameter of about 800 km; the most stressing target is a ballistic missile that must revisited at least once a second; and the SNR for a 0 dBsm target must be about 25 dB.

The element positions assumed for the Tx array are shown in Figure 22, and the associated pattern is shown in Figure 23. The beamwidth of 0.616° corresponds to an azimuth cross-beam extent of 408 km at the aforementioned range of 37,939 km. The Rx array is configured as a Y with 3-km arms of 14 sub-arrays each, plus another sub-array in the middle, to give a total of 43 sub-arrays. The azimuth beamwidth of this Rx array is 0.0145°, and the elevation beamwidth is 0.0102°. Thus, about 2566 Rx beams are required to cover the Tx beam. The azimuth cross-beam extent of the Rx beam in the theater is 9.6 km. If this azimuth extent is considered too great to give acceptable tracking accuracy, a second Rx array could be placed on the other side of the Tx array, and the target azimuth could be determined to very high accuracy by multilateration. In particular, the equations for the two ellipsoids defined by the two quasimonostatic range measurements could be solved simultaneously in the vicinity of the region bounded by the two sets of azimuth and elevation angles.

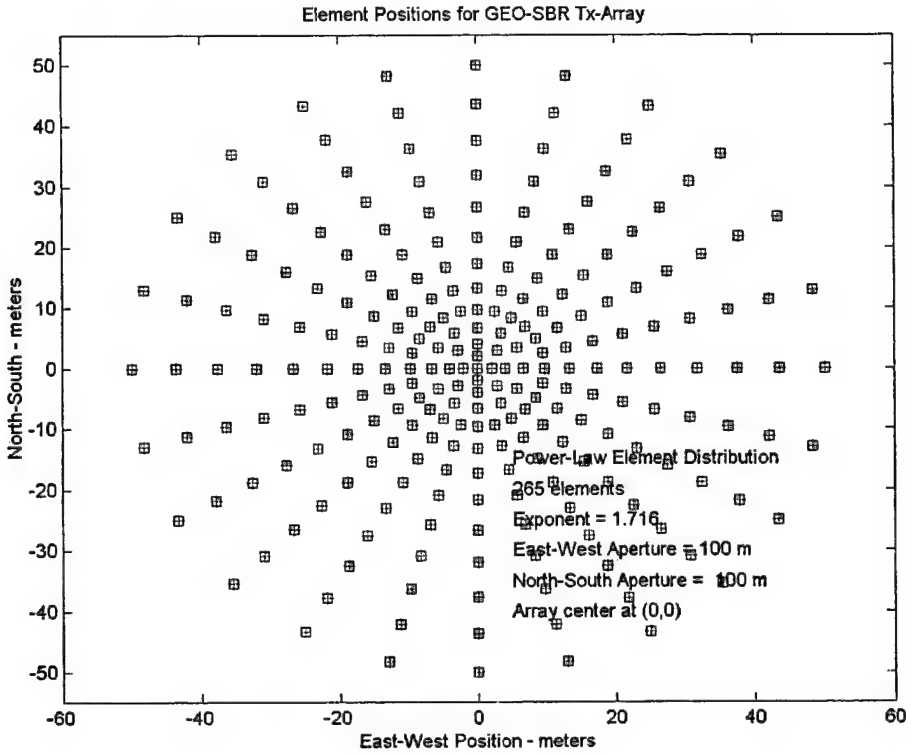

Figure 22. Element positions for the VHF/UHF GEO-SBR Tx array.

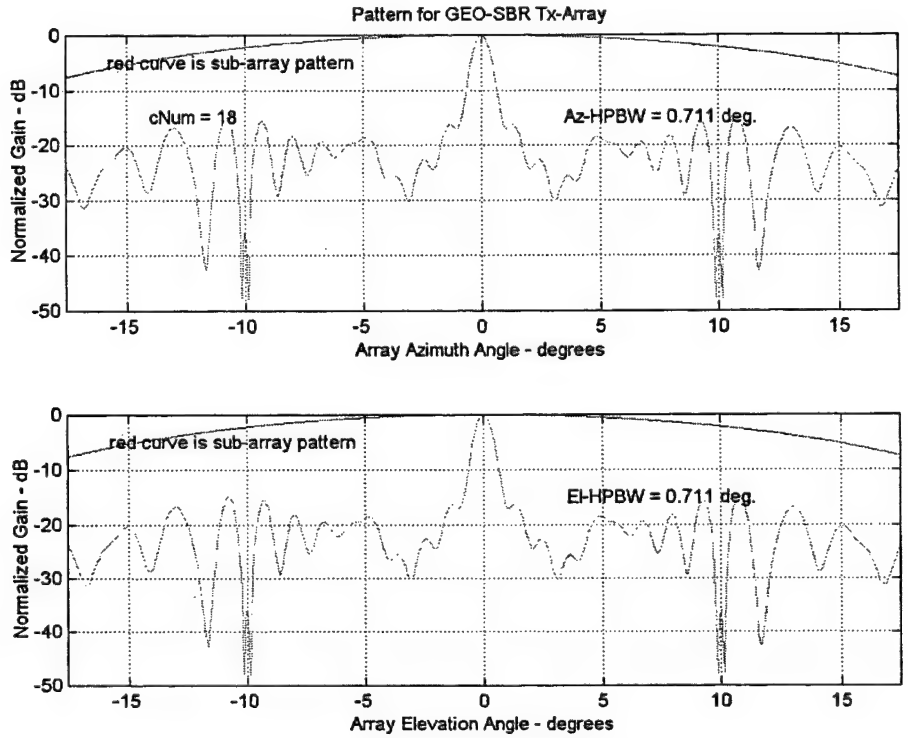

Figure 23. Pattern for the VHF/UHF GEO-SBR Tx array.

6.3 Signal Processing Implications

Because the velocities associated with the motion illustrated in Figure 21 are so small, the Doppler spread of the clutter for the VHF/UHF GEO-SBR is negligible. The MDV should be considered to be about 0.14 m/s, as determined from the minimum Doppler resolution defined by the inverse of the CIT (i. e., about 4 Hz).

The PRF for a GEO-SBR is not limited significantly by the usual need to consider range folding. Thus, a nominal value of 5 kHz is chosen simply to give a reasonable unambiguous Doppler extent for the majority of target radial velocities of interest (namely up to about Mach 3 for the assumed radar frequency band).

Because of the absence of spread-Doppler clutter, even extremely slow-moving ground vehicles can be detected and tracked using simple Doppler processing. However, there will be a need for three parallel types of processor to deal with the three different types of target, namely ground vehicles, air vehicles, and ballistic missiles. For ground vehicles, and for air vehicles with relatively small radial velocities, the full CIT of about a quarter of a second will be utilized. For air vehicles with larger radial velocities, two-dimensional spectral estimation processing will be required (Ref. 8), so that in effect sub-sets of the full CIT are processed while the targets remain in a single range cell. The FFT outputs from these sub-sets will then be non-coherently combined to achieve an acceptable detection/tracking performance. Finally, for accelerating targets like ballistic missiles, additional acceleration processing will be performed on the CIT sub-sets.

6.4 LEO-GEO System Comparisons

If the number of Tx (125) and Rx (43 or 86) sub-arrays chosen here to illustrate a feasible GEO-SBR seems too large to be considered practical, the estimate made by Pirolo and DeLap should be noted (Ref. 9). They estimated that 30 to 45 LEO SBRs are required to provide near-continuous global JSTARS-like coverage (depending on system orbit), and an additional 60 to 80 LEO-SBRs are required to provide near continuous global AWACS-like coverage. They did not address the problems caused by spread-Doppler clutter. However, they did imply that ballistic missiles could also be covered, although they do not mention whether or not additional LEO-SBRs would be required for this mission.

7. SUGGESTED FUTURE TASKS

The following tasks are suggested as possible directions for extending this study.

Develop a simulation of sparse array and MPCA processing that includes noise statistics, as well as signal, clutter, and jammer fading statistics. Extrapolate the data received during a CIT (generally 1024 pulses) using Burg's maximum entropy method (or other possible methods, as described in Ref. 8). This extrapolation will be done to give a higher spectral resolution sufficient to offset the subsequent loss of resolution caused by the windowing of the data needed to reduce the Doppler sidelobes caused by FFT processing. Use this simulation to generate illustrations of performance equivalent to the plots shown in Figures 6-8.

Add polarization as another degree of freedom to exploit for clutter-suppression and jammer suppression processing.

Evaluate the impact of orbital perturbations that may cause 3-d random variations in sparse array element positions on the antenna-beam-forming and clutter-suppression and jammer-suppression processing.

Evaluate the impact on beamforming and MPCA processing of errors in real-time measurements of element positions and in the necessary real-time phase adjustments. Include an evaluation of calibration requirements and uncertainties.

Evaluate the trade-off between sub-array size and number of elements (independent spacecraft) in the overall array.

Define an appropriate receiving, detection, and tracking system and replace the SCNR performance measure by probability of detection (P_d) and probability of false alarm (P_{fa}).

Evaluate the efficacy of MPCA processing and other possible STAP processing techniques using experimental data. If suitable SBR data can not be obtained, MCARM data (Ref. 10) may be used for this evaluation.

8. ACKNOWLEDGEMENT

I wish to thank Michael Wicks, Gerard Genello, and the Air Force Office of Scientific Research for their support, which has enabled me to perform the work reported here. I am especially grateful to Russell Brown for suggesting and assisting me with the most important technical concepts that are the basis of this work. I am also greatly indebted to Raviraj Adve and Hong Wang for the help they gave me.

9. REFERENCES

1. Brown, R. D., R. A. Schneible, H. Wang, M. C. Wicks, Y. Zhang, "STAP for Clutter Suppression with Sum and Difference Beams," *IEEE Trans. Aerospace and Elect.*, April 2000.
2. Tsandoulas, G. N., "Space-Based Radar," *Science*, pp. 257-262, 17 July 1987.
3. Lo, Y. T., Chapter 11 of the *Antenna Handbook*, Y. T. Lo and S. W. Lee, Editors, Van Nostrand Reinhold Company, New York, 1988.

*4. Jerinic, G., D. Laighton, W. Blaisdel, G. Harrell, D. Bostrom, and T. Vespa, "MODULE VALIDATION PROGRAM," RADC-TR-90-291, Final Technical Report, RADC AFSC, Griffiss AFB, NY, November 1990.

5. Andrews, G. A., and K. Gerlach, "SBR Clutter and Interference," Chapter 11 in *Space-Based Radar Handbook*, L. J. Cantafio, Editor, Artech House,Norwood, MA, 1989.

*6. Zhang, Yuhong, and Braham Himed, "Bistatic Space-Time Adaptive Processing (STAP) for Airborne/Spaceborne Applications," Final Technical Report, AFRL-SN-RS-TR-1999-97, Stiefvater Consultants, Rome, NY, May 1999.

7. Analytical Graphics, Inc., 325 Technology Drive, Malvern, PA 19355, http://www.stk.com.
8. Marple, S. L., Jr., *Digital Spectral Analysis with Applications*, Prentice-Hall, Inc., Englewood Cliffs, NJ, 1987.
9. Pirolo, David G., Major, USAF, HQ AFSPC/XPX, and Captain Ronald A. DeLap, USAF SMC/XRT, "Space-Based Moving Target Indicator System Roadmap," Draft Document, 2 February 1998.

*10. Sloper, Dave, Dave Fenner, Jim Arntz, and Ed Fogle, "Multi-Channel Airborne Radar Measurement (MCARM)," RL-TR-96-49, Four Volumes, Final Technical Report, Rome Laboratory, AFMC, Rome, NY, April 1996.